Supplementary Material:

Observations and simulations of new snow density in the drifting snow dominated environment of Antarctica

Nander WEVER, Eric KEENAN, Charles AMORY, Michael LEHNING, Armin SIG-MUND, Hendrik HUWALD, Jan T. M. LENAERTS
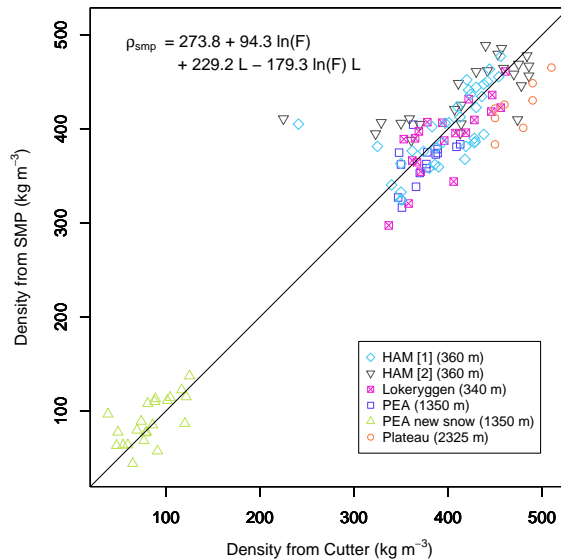
Figure S1: Calibration of the SnowMicroPen (SMP) using density cutter measurements in snow profiles and new snow accumulations. Different marker types and colours indicate the different snowpits. The equation shows the calibration fit for ρ_{smp} as a function of the median force F and element length L.

S1   Calibration of SnowMicroPen

In the field, we used a SnowMicroPen (SMP) version 4 to survey the snow microstructure. Since this SMP version is newer than the one used for the calibration developed by Proksch and others (2015) and was operated by us with different settings, we compared SMP measurements with manual density observations in snow pits. Two snow pits were taken near the summit of Hammarryggen (HAM, ice rise at 70.502°S, 21.873°E), one near the summit of Lokeryggen (an ice rise east of HAM at 70.536°S, 24.072°E, approximately 340 m a.s.l.), one at PEA (71.939°S, 23.315°E) and one at the Plateau about 30 km South of PEA on the South side of the Sør Rondane mountains at an elevation of about 2325 m a.s.l. (72.258°S, 23.245°E).

For this comparison, first a couple of SMP measurements were taken along a line that would form the later snow pit wall. After the SMP measurements, the snowpit was dug, as close as possible to the SMP locations allowing for a direct comparison between manual snow measurements and the SMP. The manual snow density measurements were taken using a 100 cm³, 3 cm high box cutter (see Proksch and others, 2016, for details), resulting in a density profile in steps of 3 cm.

On 3 days in December 2016, fresh snowfall at PEA allowed for SMP measurements of light snow with densities below 100 kg m^{-3}. In these cases, only the new snow layer, which was on top of a hard old snow layer, was surveyed by inserting the box cutter vertically in the new snow layer and using a measurement of new snow depth at the location of the box cutter to calculate density.

The average SMP force and element size over the same segments as in the observations was determined and used to fit the equation as used in Proksch and others (2015). Fig. S1 shows the result of the calibration. The residual standard error is 37 kg m^{-3}. Uncertainties are related to three factors: (i) the locations of the density cutter and SMP measurements are at least a few cm, up to 30 cm, apart (ii) the uncertainty for box density cutters is substantial, but generally estimated to be less than 9% (Conger and McClung, 2009; Proksch and others, 2016), and (iii) inherent discrepancies between the relationship between force and element length from SMP and snow density.

S2 Terrestrial Laser Scanning

Surface topography maps were obtained using a Riegl VZ-6000 (Riegl, 2017) Terrestrial Laser Scanner. The VZ-6000 laser wavelength is 1064 nm, which is in the near infrared range and provides high reflectivity on snow and ice surfaces (Prokop and others, 2008). More details on accuracy and processing of the scans near PEA can be found in Sommer and others (2018). For the scans at HAM, we followed similar procedures as at PEA. By using reflectors installed on bamboo poles, scans were registered with respect to the reflectors, such that the difference between two successive scans reveals the spatial patterns of erosion and deposition of snow. We used multiple scan positions to create one combined point cloud. After applying a 10 cm octree filter on the point cloud, a 3D surface was obtained. By walking along fixed corridors, disturbance of the snow is limited. From the installed reflectors, 4 reflectors could be used over the full period. The scan accuracy is generally higher within the area enclosed by the reflectors.

S3 MERRA-2 Wind Speed Evaluation

We evaluated MERRA-2 wind speed for sites with available observations, as listed in Table S1. Fig. S2 compares the daily average observed wind speed corrected to 10 m height with MERRA-2 wind speed for D17, D47 and PEA. For the measurement period at D17, average observed and MERRA-2 wind speed is 11.7 m s^{-1} and 10.4 m s^{-1}, respectively. Similarly, average observed and MERRA-2 wind speed at D47 is 13.9 m s^{-1} and 13.4 m s^{-1}, respectively. Sites D17 and D47 have a similar range of daily average wind speed, ranging from close to 0 m s^{-1} to maximum values of 32 m s^{-1} and 30 m s^{-1} for D17 and D47, respectively. The average wind speed is higher at D47 (13.9 m s^{-1}) than at D17 (11.7 m s^{-1}). MERRA-2 wind speed covers the range in daily average wind speed well for these sites. We find that MERRA-2 provides a better agreement with observations for D47 ($r^2 = 0.87$, $p < 0.001$) than for D17 ($r^2 = 0.66$, $p < 0.001$). The root-mean-squared error (RMSE) is also correspondingly smaller for D47 (1.53 m s^{-1}) than for D17 (3.17 m s^{-1}). For D17, significant lower correspondence is found for days without precipitation than with precipitation (Fig. S2a), determined using the statistical tool `cocor` (Diedenhofen and Musch, 2015). Particularly, higher wind speeds on days without precipitation are underestimated by MERRA-2. For D47, the r^2 value is similar for days with and without precipitation in MERRA-2 (Fig. S2b).

For the PEA site, we also have in-situ wind speed observations from the drift stations (Fig. S2c). Since the surroundings of PEA are heterogeneous, and due to

Table S1: Data sources for simulations run using in-situ wind data, and precipitation bias corrections applied in all simulations

When	Correction applied
D17	
2010-02-03T12:30 − 2018-12-31T23:30	In-situ wind from blowing snow mast
2014-01-01T00:00 − 2014-01-29T00:00	MERRA-2 precipitation multiplied by 3[1]
D47	
2010-01-09T16:30 − 2012-12-27T10:30	In-situ wind from blowing snow mast
PEA	
2009-02-02T19:30 − 2016-12-11T12:30	In-situ wind from IMAU AWS mast
2016-12-10T00:00 - 2016-12-28T00:00	MERRA-2 precipitation multiplied by 3[1]
2016-12-28T00:00 - 2017-01-15T00:00	MERRA-2 precipitation multiplied by 9[1]
2016-12-11T12:30 − 2017-12-22T11:30	In-situ wind from blowing snow mast[2]
2017-12-22T11:30 − 2019-01-17T21:30	In-situ wind from IMAU AWS mast
HAM	
2018-12-10T00:00 − 2019-01-15T00:00	MERRA-2 precipitation multiplied by 3

[1] This correction is applied in all simulations.

[2] From 2017-01-12T14:30 onward, this data source has some more extensive data gaps, for which data from the IMAU AWS mast is used.

the sheltered location of the site, the local wind climate is poorly represented by the approximately 23 km x 56 km grid spacing along latitudinal and longitudinal direction, respectively, of MERRA-2 in this area. For the two week overlapping period with in-situ wind speed observations, average observed wind speed transformed to 10 m was 5.1 m s^{-1}, whereas MERRA-2 simulated 11.1 m s^{-1}. We find that at lower observed wind speeds (less than 5 m s^{-1}), the discrepancies with MERRA-2 simulated wind speed are much higher in absolute and relative sense compared to the higher observed wind speed regime. The worse correspondence between MERRA-2 and observations compared to sites D17 and D47 is indicative of the influence of the very variable surroundings of PEA.

Fig. S3 shows the same figure as Fig. S2, but for half-hourly data. On half-hourly timescales, the RMSE generally increases, while particularly for the periods without precipitation in MERRA-2, the r^2 values decrease substantially. Fig. S3a also clearly shows that high wind speeds observed in the absence of precipitation are underestimated by MERRA-2 at D17, whereas at PEA, the spread in the low observed wind speed regime is substantial.

For HAM, we lack in-situ weather observations. The closest MERRA-2 grid point has an elevation of 88 m a.s.l, whereas the HAM field site was at the top of the ice rise, at approximately 360 m a.s.l. As shown by Lenaerts and others (2014), the ice rises form an area with high variability in climate conditions, and winter air temperatures on top of the ice rise were found to be higher than on the surrounding ice shelves. Wind speed around the ice rises is also variable due to dynamical processes in the atmosphere. The findings suggest that without in-situ data from the study site, simple bias corrections for MERRA-2 output would not suffice and we used the MERRA-2 data as-is, including for temperature and wind speed.
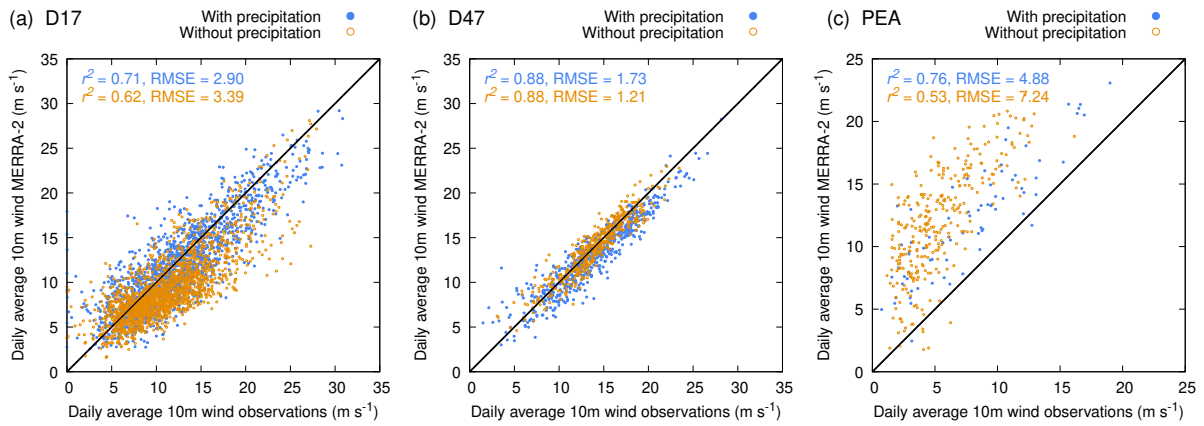
Figure S2: Scatter plots comparing bias-corrected daily average wind speed from MERRA-2 with in-situ observed wind speeds transformed to 10 m height for sites (a) D17, (b) D47, and (c) PEA. Different colours and markers are used for days with precipitation and without precipitation in MERRA-2. The solid black line denotes the 1:1 line and RMSE denotes the Root Mean Square Error.
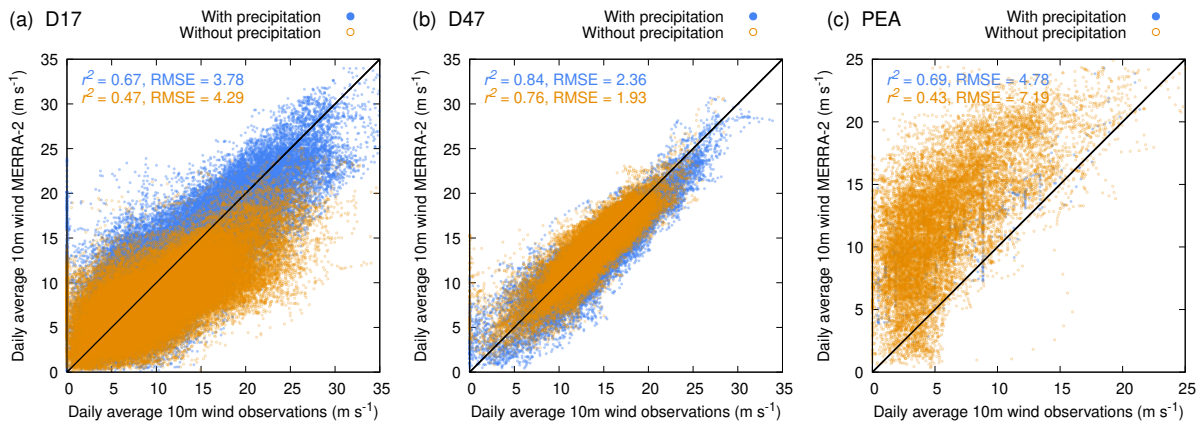

Figure S3: Scatter plots comparing bias-corrected half-hourly wind speed linearly interpolated from hourly MERRA-2 with in-situ observed wind speeds transformed to 10 m height for sites (a) D17, (b) D47, and (c) PEA. Different colours are used for periods with and without precipitation (defined as less than 0.024 $kg\,m^{-2}\,day^{-1}$) in MERRA-2. The solid black line denotes the 1:1 line and RMSE denotes the Root Mean Square Error.

S4   Daily Sums of Drifting Snow

Fig. S4 compares the daily sums of observed drifting snow mass transport with the daily sums of simulated saltation mass transport for the three sites D17, D47 and PEA. Fig. S5 compares the daily sums of observed drifting snow mass transport with the daily sums of simulated saltation mass transport for the three simulation setups, and for sites D17 and D47.
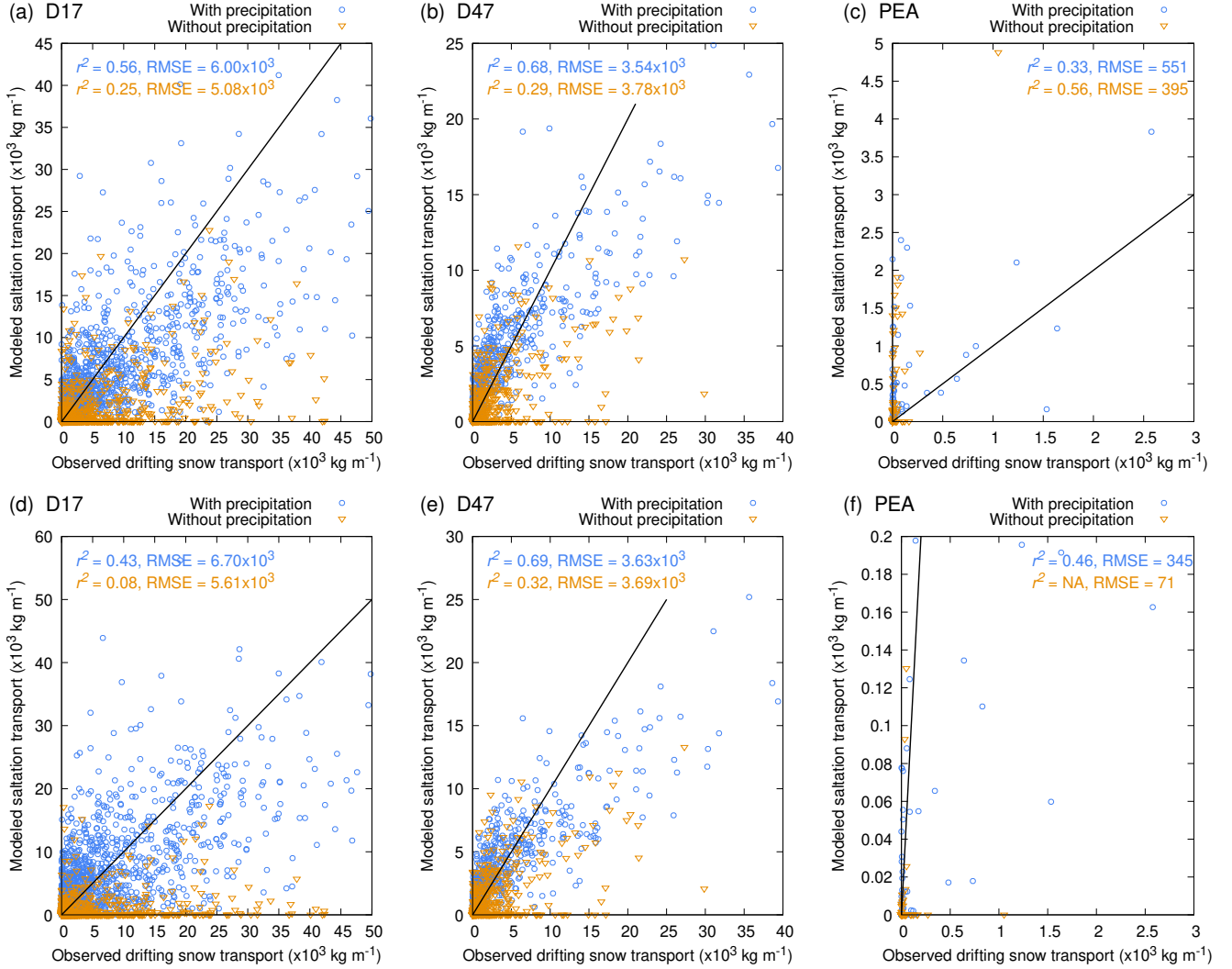
Figure S4: Scatter plots showing daily sums of observed drifting snow mass transport versus SNOWPACK simulated saltation mass transport using the redeposit scheme for sites (a, d) D17, (b, e) D47, and (c, f) PEA. In (a, b, c), in-situ observed wind speed was used for the simulations and in (d, e, f) MERRA-2 wind speed was used for the simulations. Different colours and markers are used for days with and without precipitation (defined as less than 0.024 kg m^{-2} day^{-1}) in MERRA-2. The solid black line denotes the 1:1 line and RMSE denotes the Root Mean Square Error and in (f), "NA" denotes that the r^2 value was not significant at $p < 0.001$. Note that zero values are also plotted.
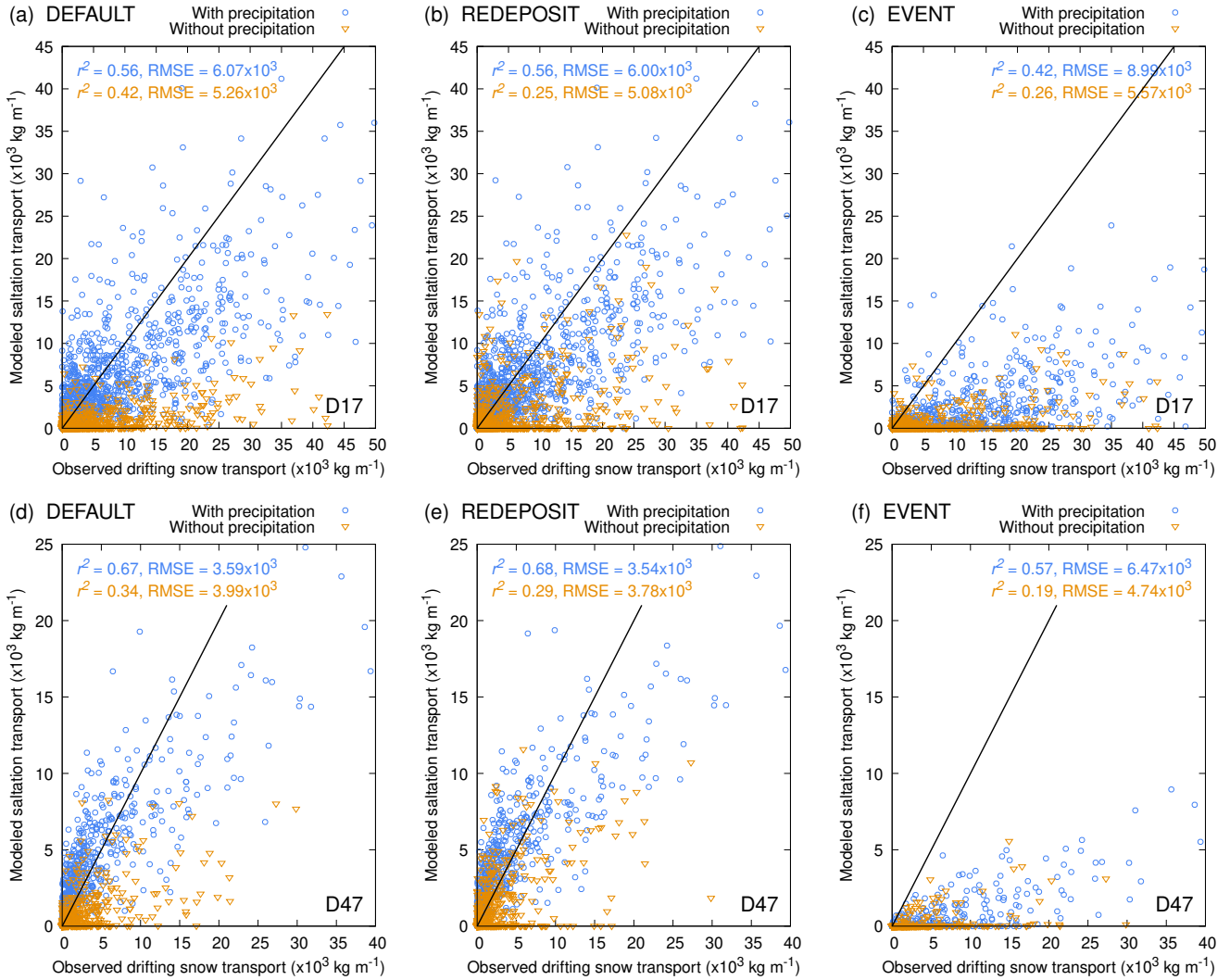
Figure S5: Scatter plots showing daily sums of observed drifting snow mass transport versus SNOWPACK simulated saltation mass transport using the (a, d) default scheme, (b, e) redeposit scheme and (c, f) the event-driven scheme for sites (a, b, c) D17, (d, e, f) D47, using in-situ observed wind speed. Different colours and markers are used for periods with and without precipitation (defined as less than 0.001 kg m^{-2} day^{-1}) in MERRA-2. The solid black line denotes the 1:1 line and RMSE denotes the Root Mean Square Error. Note that zero values are also plotted.
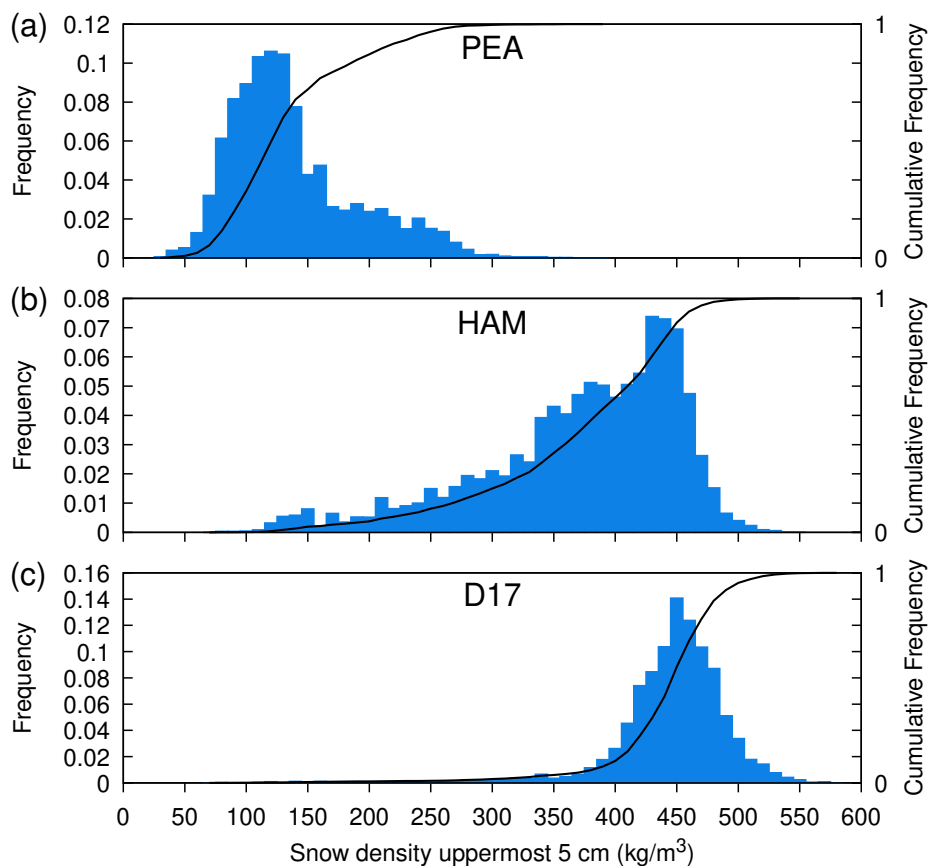
Figure S6: Relative distributions of the frequencies (bars, left axis) and cumulative frequencies (solid black lines, right axis) of simulated snow density in the uppermost 5 cm of the firn layer, for (a) PEA, (b) HAM and (c) D17. Data was binned with bin widths of 10 kg m^{-3} wide bins.

S5   Simulated Surface Snow Density Distributions

Fig. S6 shows the distributions of simulated snow density in the uppermost 5 cm of the firn layer for the period 2010-2019, for the simulation from PEA, HAM and D17, respectively. Note that simulated density at PEA is likely underestimated in this particular simulation setup, since the bias corrected MERRA-2 wind speed underestimates the highest wind speeds (see Figs. S2c and S3c).

References

Conger SM and McClung DM (2009) Comparison of density cutters for snow profile observations. *J. Glaciol.*, **55**(189), 163–169 (doi: 10.3189/002214309788609038)

Diedenhofen B and Musch J (2015) cocor: A comprehensive solution for the statistical comparison of correlations. *PLOS ONE*, **10**(4), 1–12 (doi: 10.1371/journal.pone.0121945)

Lenaerts JT, Brown J, Van Den Broeke MR, Matsuoka K, Drews R, Callens D, Philippe M, Gorodetskaya IV, Van Meijgaard E, Reijmer CH and et al (2014) High variability of climate and surface mass balance induced by Antarctic ice rises. *J. Glaciol.*, **60**(224), 1101–1110 (doi: 10.3189/2014JoG14J040)

Prokop A, Schirmer M, Rub M, Lehning M and Stocker M (2008) A comparison of measurement methods: terrestrial laser scanning, tachymetry and snow probing for the determination of the spatial snow-depth distribution on slopes. *Ann. Glaciol.*, **49**, 210–216 (doi: 10.3189/172756408787814726)

Proksch M, Löwe H and Schneebeli M (2015) Density, specific surface area, and correlation length of snow measured by high-resolution penetrometry. *J. Geophys. Res.*, **120**(2), 346–362 (doi: 10.1002/2014JF003266)

Proksch M, Rutter N, Fierz C and Schneebeli M (2016) Intercomparison of snow density measurements: bias, precision, and vertical resolution. *The Cryosphere*, **10**(1), 371–384 (doi: 10.5194/tc-10-371-2016)

Riegl (2017) *RIEGL VZ-6000 Datasheet*

Sommer CG, Wever N, Fierz C and Lehning M (2018) Investigation of a wind-packing event in Queen Maud Land, Antarctica. *Cryosphere*, **12**(9), 2923–2939 (doi: 10.5194/tc-12-2923-2018)